



HAL
open science

Dissociative Recombination of Acetone Fragments, Adducts, and Dimer Ions

Suliman Al Shammari, Guilherme C. Almeida, Maria Luiza M. Rocco,
Jean-Luc Le Garrec, James Brian Alexander Mitchell

► **To cite this version:**

Suliman Al Shammari, Guilherme C. Almeida, Maria Luiza M. Rocco, Jean-Luc Le Garrec, James Brian Alexander Mitchell. Dissociative Recombination of Acetone Fragments, Adducts, and Dimer Ions. *Journal of Physical Chemistry A*, 2017, 121 (21), pp.4114-4122. 10.1021/acs.jpca.7b00987 . hal-01580446

HAL Id: hal-01580446

<https://univ-rennes.hal.science/hal-01580446>

Submitted on 16 May 2018

HAL is a multi-disciplinary open access archive for the deposit and dissemination of scientific research documents, whether they are published or not. The documents may come from teaching and research institutions in France or abroad, or from public or private research centers.

L'archive ouverte pluridisciplinaire **HAL**, est destinée au dépôt et à la diffusion de documents scientifiques de niveau recherche, publiés ou non, émanant des établissements d'enseignement et de recherche français ou étrangers, des laboratoires publics ou privés.

The Dissociative Recombination of Acetone Fragments, Adducts and Dimer Ions

*Suliman Al Shammari^{†‡}, Guilherme C. Almeida[§], Maria Luiza M. Rocco^{§3}, Jean-Luc Le Garrec[‡]
and J. Brian A. Mitchell^{*‡}*

[‡]Institut de Physique de Rennes, U.M.R du C.N.R.S. No. 6451, Université de Rennes I, 35042,
Rennes, France

[†]King Abdulaziz City for Science and Technology, P.O. Box 6086, Riyadh, 11442, Saudi Arabia

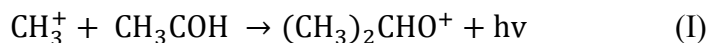
[§] Instituto de Química, Universidade Federal do Rio de Janeiro, Rio de Janeiro, RJ, Brazil.

ABSTRACT: The room temperature dissociative recombination of ions formed in an acetone/argon plasma has been studied using the Flowing Afterglow Langmuir Probe-Mass Spectrometer method. By changing the concentration of acetone density, it is possible to have a plasma dominated by different types of ions (fragments, adducts and dimer ions). The application of these measurements to astrophysical plasmas is discussed.

1. Introduction:

Dissociative recombination (DR) is the reaction in which a molecular ion recombines with an electron and dissociates into neutral fragments. General reviews on this reaction have been given by several authors such as Florescu-Mitchell and Mitchell¹, Larsson and Orel² and Adams and co-workers³. This process plays a major role in industrial processing and nuclear fusion plasmas as well as in the evolution and composition of interstellar gas clouds and planetary ionospheres.

Neutral acetone (CH₃COCH₃) was first detected in the interstellar medium (ISM) by Combes et al,⁴ inside a hot core of the Sgr B2 molecular cloud and few years later by Friedel et al,⁵ in the Orion-KL star-forming region. The first suggested mechanism to explain interstellar acetone involved a radiative association reaction followed by a DR reaction as shown below:



Herbst, Giles and Smith⁶ showed that, based on laboratory measurements and theoretical calculations, this mechanism was in fact too slow to explain the high abundances of acetone observed in these star-forming regions. Further work⁷⁻⁸ suggested that an ice phase chemistry involving carbon, oxygen and hydrogen on the surface of CO ice coated interstellar grains could produce molecules such as formaldehyde (CH₃COH) and methanol which, when protonated, can react by alkyl cation transfer, followed by a DR reaction, to produce neutral acetone according to reactions III and IV.



Although there is no consensus as to whether the acetone observed in interstellar clouds is produced directly from gas phase components or requires the evaporation of ice phase components seeded by the interstellar grains, there is no doubt that DR is the key process for obtaining large neutral organic molecules like acetone in the ISM.

In order to provide basic data for a better understanding on the formation of interstellar and circumstellar acetone, we have performed a series of measurements to determine the DR rates of its ions. A key feature of the Rennes FALP-MS apparatus is that because it has a movable mass spectrometer, the decay of several different ions can be followed as they drift through a flow tube and their individual recombination rates can be determined. This is different from other Flowing afterglow apparatuses⁹⁻¹² which require that the afterglow contains only a single ion species and where the recombination rate is derived simply by studying the decay of the afterglow electrons using Langmuir Probe Measurements. Thus in this case we have been able to study the electron recombination of the parent ion (CH₃COCH₃⁺) as well as that of the major fragment CH₃CO⁺ and of the adduct ions CH₃COCH₃.CH₃⁺, CH₃CO-CH₃.CH₃CO⁺ and the dimer ion (CH₃COCH₃)₂⁺.

These adduct ions should also be present inside the hot cores of dense interstellar clouds where acetone is abundant. Almeida et al.¹³ derived the destruction cross section of ice phase acetone in a synchrotron irradiation experiment. The authors concluded that if the photon flux is sufficiently high in an ISM environment, the acetone ice phase can be effectively decomposed and this will seed the gas phase environment with acetone molecules and its derivatives such as its adducts, which will provide a path for the development of a gas phase organic chemistry leading to the complex organic molecules that have been measured inside these hot cores.

2. Experimental Method

2.1 Overview of FALP technique

The Flowing Afterglow (FA) technique was first developed for the study of ion-molecule reactions by Ferguson and co-workers¹⁴. The basic concept of this apparatus is that the concentration of an active species can be tracked as a function of distance along a tube through which gas flows with a constant velocity. This distance can thus be converted to time and so rate coefficients for chemical reactions can be determined. A significant development of the FA was

the introduction by Adams and Smith¹⁵ of a movable Langmuir Probe (LP) for measurements of electron density and temperatures along the flow tube¹⁶. The probe method provides absolute values of electron concentration at a given position. Thus the Flowing Afterglow with Langmuir probe (FALP) technique could be used for the direct measurement of the dissociative recombination (DR) rate coefficients of studied ions by tracking the decay of the electron concentration along the flow. Generally speaking, the major limitation of this implementation has been that only one ion could be present in the afterglow during the measurements as it was considered that the concentration of this positive ion is equal to the concentration of the negative electrons so that plasma neutrality is maintained. In a recent article however, by Fournier et al.¹⁷ DR rate coefficients have been measured in a flowing afterglow apparatus (VENDAMS) where the plasma contained many ions, using a method based on plasma modelling to obtain the individual recombination rate coefficients. In our case, the single ion limitation was overcome with the development of the flowing afterglow apparatus by Rowe and co-workers at the University of Rennes^{18,19} which employs a movable mass spectrometer to track the concentration of individual ions along the flow. Thus measurements of DR rate coefficients, α , in those situations where several ions are simultaneously created, become possible. The apparatus used in this technique is called the flowing afterglow Langmuir probe mass spectrometer (FALP-MS) and this is illustrated in Figure 1.

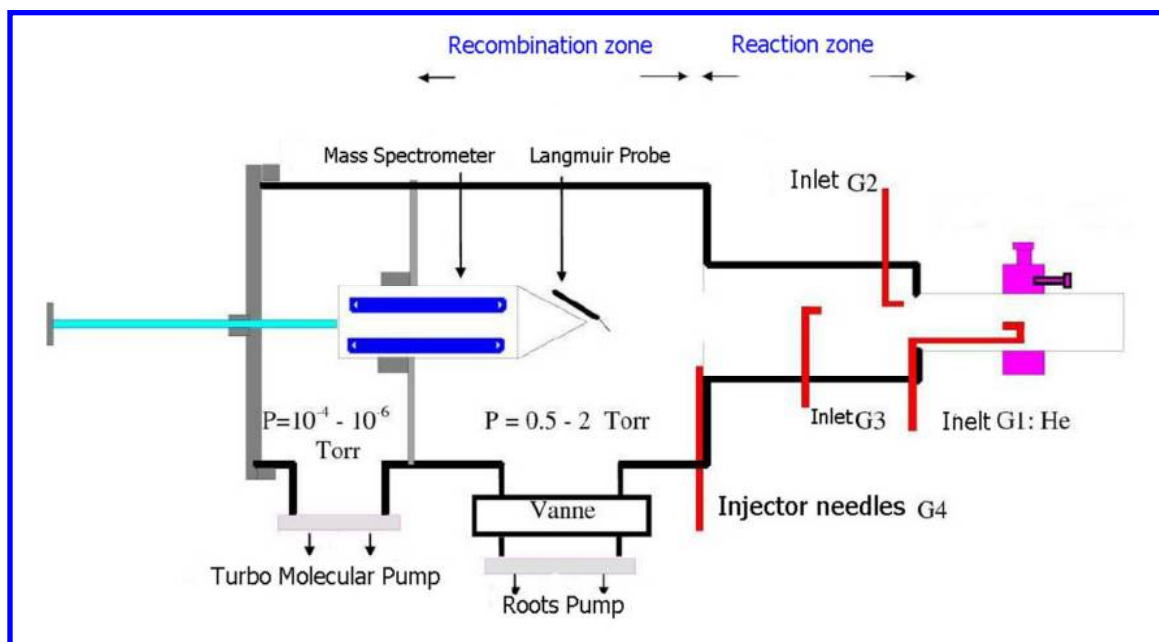


Fig. 1: Sketch of FALP-MS apparatus at University of Rennes²⁰.

In the present version of the FALP-MS, pure helium buffer gas flows through a 4.2 cm diameter glass tube (G1) and is ionized in a microwave cavity operating at 2.45 GHz to form a plasma containing of He^+ , He_2^+ ions, metastable helium He^m and electrons. The electrons are quickly thermalized down to room temperature by helium buffer gas collisions²¹. The plasma is then

driven by the buffer gas through a stainless steel flow tube with an inner diameter of 4 cm. There are several reactant gas inlets at different positions along the flow tube (G2, G3, and G4). The He^m are destroyed by introducing some Argon gas through the second entry port (G2) into the afterglow, thus creating Ar^+ ions and more electrons by Penning ionization:



The He^+ ions react with He neutral atoms to produce He_2^+ ions which also react with the Ar gas to produce Ar^+ ions which, in turn will be used to produce the ion to be studied, by reaction with its parent gas. He_2^+ ions are removed by reaction (VII):

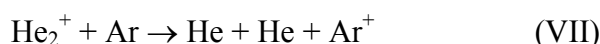


Table 1 lists the reactions (and their corresponding reaction rate coefficients) involved in the initial plasma formation and its conversion to an argon plasma. The rates are taken from ref. 22.

Reaction	Rate Coefficient ($cm^3 s^{-1}$)
$He^+ + He + He \rightarrow He_2^+ + He$	1×10^{-31}
$He^m + He^m \rightarrow He^+ + He + e^-$	5×10^{-9}
$\rightarrow He_2^+ + e^-$	5×10^{-9}
$He_2^+ + e^- \rightarrow 2He$	$< 3 \times 10^{-10}$
Ar	
$He^+ + Ar \rightarrow Ar^+ + He$	1×10^{-13}
$He^m + Ar \rightarrow He + Ar^+ + e$	7×10^{-11}
$He_2^+ + Ar \rightarrow He + He + Ar^+$	2×10^{-10}

It should be noted that He^+ ions react very slowly with argon¹⁵ and that the likelihood of forming argon metastable atoms in any of these reactions is very small. The great advantage of helium as a buffer gas is to ensure that hot electrons created in the microwave discharge, are quickly cooled by electron-atom collisions so that one obtains the same temperature in the afterglow for both ions and neutrals ($T_{gas} = T_{ions} = T_{electrons}$).

Figure 2 shows the mass spectrum taken in the present experiment after injection of argon into the helium plasma. The absence of He_2^+ in the mass spectrum (in the measurement area, about 1 cm after the argon injection through the second entry port G2) indicated that reaction (VII)

had gone to completion, prior to arriving at the measurement region and from this, knowing the rate for reaction (V), one could be sure that all helium metastable atoms had also been converted.

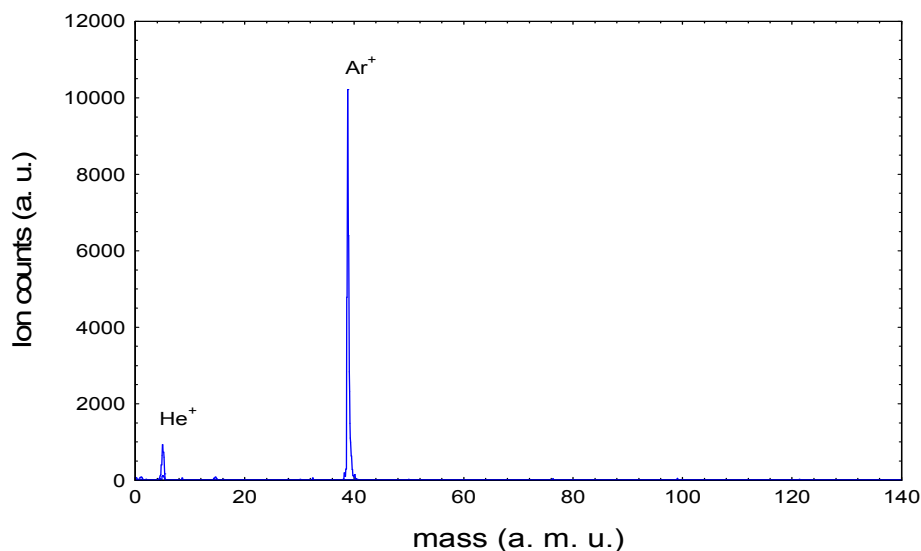


Fig. 2 Mass Spectrum taken 1 cm after the eight- needles port with *Ar* gas injected into the *He* afterglow. The electron density in the plasma was typically $3.20 \times 10^9 \text{ cm}^{-3}$ for this measurement performed at 0.54 Torr.

Acetone vapor CH_3COCH_3 was introduced into the flow at different flow rates via a third port (G4, needles entry) that consists of eight hypodermic needles that inject gas into the center of the plasma without disturbing the aerodynamics of the flow. As will be seen later, a variety of ions were formed with their relative concentrations depending upon the flow rate of the mixture and thus the number density of acetone molecules in the flow.

2.2 Data analysis

Under these experimental conditions, i.e. 0.54 Torr, room temperature (300 K) and typically 10^{10} electrons per cm^3 , Ar^+ ions are reacted away within a short distance downstream of the CH_3COCH_3 injection. The measurements of the electron-ion recombination rate coefficient can be performed using one of three methods²³. In this paper, we shall investigate these three methods and compare the results obtained using acetone as the parent molecule.

For a plasma containing a single positive ion that does not react with the neutral gas, the recombination process dominates and the electron density decay with time, t , can be written as:

$$\frac{dn_e}{dt} = -\alpha n_e n_+ \quad (1)$$

where α is the recombination rate coefficient and n_e, n_+ are the electron and ion densities. Assuming that the $n_e = n_+$ (the plasma is neutral and does not contain negative ions), the equation (1) can be re-written as:

$$\frac{dn_e}{dt} = -\alpha n_e^2 \quad (2)$$

By using the Langmuir Probe (LP), the electron density at several positions in the flowing afterglow can be measured. Equation (2) can then be written in terms of the downstream distance, z , and the flow velocity, v :

$$v \frac{dn_e}{dz} = -\alpha n_e^2 \quad (3)$$

Integrating equation (3) from the origin, $z_0 = 0$ (taken as the position of the needles entry port G4), to some downstream position z , yields the following expression for n_e :

$$\left(\frac{1}{n_e}\right)_z = \left(\frac{1}{n_e}\right)_0 + \frac{\alpha}{v} z \quad (4)$$

The plot of $1/n_e$ vs z , allows us to determine the recombination rate coefficient α if the flow velocity v is known. In the following, this method for measuring recombination rate coefficients shall be referred to as the single-ion method.

This method has been used during the course of these experiments with O_2^+ ion as a systematic, standard measurement to test the FALP-MS apparatus. The recombination rate coefficient for O_2^+ was found to be $2.01 \times 10^{-7} \text{ cm}^3 \text{ s}^{-1}$ and this value is in very good agreement with accepted value¹ for this ion ($2.0 \times 10^{-7} \text{ cm}^3 \text{ s}^{-1}$).

The second method to determine the recombination coefficient rate is when the plasma contains several ions, as in our case, during the measurements of the recombination coefficient rate for acetone ions. One can write down the equation for the change in the density $[M^+]$ of the ions under study, as a function of time, t , and therefore of distance, along the flow tube:

$$\frac{d[M^+]}{dt} = v \frac{d[M^+]}{dz} = \text{Production terms} - \alpha [M^+]n_e - k[M^+][X] - \frac{D_A[M^+]}{\Lambda^2} \dots \quad (5)$$

where v is the flow velocity which was $1.85 \times 10^4 \text{ cm/s}$ in our measurements, $[X]$ denotes the density of reactant gas present in the plasma reacting at the rate constant, k , D_A is the coefficient of ambipolar diffusion and Λ is the characteristic diffusion length. The flow velocity can be measured by pulse modulating the microwave discharge and determining the time of flight of the electron pulse so produced, between the source and a downstream detector (Langmuir probe).

The production terms have generally been ignored in our past measurements²³ considering that the ions we studied were produced during the titration process in which the argon ions dominating the plasma were totally converted into monomer ions whose recombination was then studied. Thus in this case one could ignore the production terms and so by integrating equation (5) from some initial starting point, z_0 to some position, z , one obtains the following solution:

$$v \ln \frac{[M^+]_z}{[M^+]_{z_0}} = -\alpha \int_{z_0}^z n_e dz - \left\{ k[X] + \frac{D_A}{\Lambda^2} \right\} (z - z_0) \dots \quad (6)$$

where $[M^+]_z$ and $[M^+]_{z_0}$ are the ion densities at position z and z_0 , respectively. As can be seen, a plot of the left-hand side of equation (6) versus $\int n_e dz$ yields α .

It can also be seen from equation (6) that when ion-molecule reactions and diffusion losses are small compared to those due to recombination, one can measure both $[M^+]$ and n_e , at various z values from some initial starting point, z_0 to the point where the measurement is made for a given initial electron density $n_e(0)$. It should be noted that this analysis supposes that the parent gas does not undergo electron attachment reactions. This is the case for acetone²⁴. This method is referred to in the following as the multiple ion/ z variable method.

If ion-molecule reactions are not negligible, M^+ ions react with the parent gas to produce other ions. M^+ ions may also be continuing to be produced by ion-molecule reactions. We shall see that this is the case in the present study and we can extend equation 6 to include the production term for a particular case, assuming that the ratio $[A^+]/[M^+]$ remains approximately constant, thus:

$$v \ln \frac{[M^+]_z}{[M^+]_{z_0}} \sim k_1 \frac{[A^+][X]}{[M^+]} (z - z_0) - \alpha \int_{z_0}^z n_e dz - \left\{ k_2[X] + \frac{D_A}{\Lambda^2} \right\} (z - z_0) \dots \quad (7)$$

Where $[A^+]$ is the ion responsible for the formation of M^+ with reaction rate k_1 and k_2 is the rate of destruction of M^+ by ion molecule reaction.

It is still possible however to use equation (7) to determine α , by measuring the ratio on the Left Hand Side (LHS) but at a fixed value of z for different electron densities. Indeed, the ion molecule reactions which produce and destroy M^+ do not depend on the electron density but only on the density of the reactant gas and the time, i.e. the position z in the reaction zone. Varying the electron density in the flow can be achieved in practice, by varying the position of the microwave cavity with respect to helium inlet port (G1). In this method, the production and loss terms on the RHS involving ion-molecule reactions are now constant (being independent of electron density) and only reactions involving electrons are taken into consideration. (In practice the electron density is not varied greatly and so one can ignore any change in the diffusion term). Therefore, assuming that electron attachment does not occur in this chemical reaction network, only dissociative electron recombination plays a role in the evolution of both the ions and electron density. As a consequence, this analysis is well suited to the determination of the dissociative recombination rate coefficient of ions which are not terminal, electron density being the only variable parameter. This method is referred to in the following as the multiple ion/fixed z method.

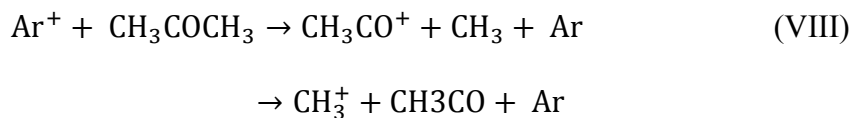
Systematic errors in the measurement arise primarily due to two factors. Firstly, the determination of the exact length of the Langmuir probe (and thus of the electron density) is subject to an uncertainty of a 10% and secondly the measurement of the flow velocity is accurate to within $\pm 15\%$. Other errors associated with the measurement of the ratio of the ion density at different distances along the flow are primarily statistical in nature and are quoted in the results below. Taking these factors into account, one can say that the combined systematic and statistical uncertainty in the quoted values for the rate coefficients presented in this paper is $\pm 30\%$.

3 Results and discussion

The ion spectra obtained depend on acetone density in the flow because the ions initially formed can react with the parent gas to form other ions, adducts and at high acetone concentration, the dimer. Thus, unlike in previous experiments performed with this apparatus, the ions in the flow are generally not terminal ions and so the analysis has to suit the appropriate situation as discussed above. The following subsections describe the physical chemistry processes, as a function of acetone density, introduced into the plasma.

3.1 Low acetone density

In the experiment, acetone vapor was diluted with helium gas in a ratio of 1:20, and it was introduced into the argon plasma, via the eight-needle entry port. Figure 3 shows the mass spectrum obtained 30 mm downstream from the entry port. In this example, the acetone was injected with a rather low flow rate ($50 \text{ cm}^3 \text{ min}^{-1}$) into the argon plasma so as to produce an acetone density of $3.2 \times 10^{12} \text{ molecules cm}^{-3}$, the initial electron density being $7.91 \times 10^9 \text{ cm}^{-3}$. It can be seen that there are two principle ions appearing in the reaction zone of the FALP-MS apparatus, these being CH_3^+ ($m/z = 15$) and acetyl cations CH_3CO^+ ($m/z = 43$) formed by reactions VIII [24], along with a remnant of Ar^+ . Thus, it is seen that reaction VIII is the dominant ion formation process at this acetone density:



It appears that the direct formation of the acetone parent ion is negligible. It should be noted here that other smaller peaks also appear at higher mass numbers indicating the presence of limited further reaction. Neither these nor evidence of residual Ar^+ were seen further downstream, indicating that at this acetone density, production and ion-molecule loss processes can be neglected.

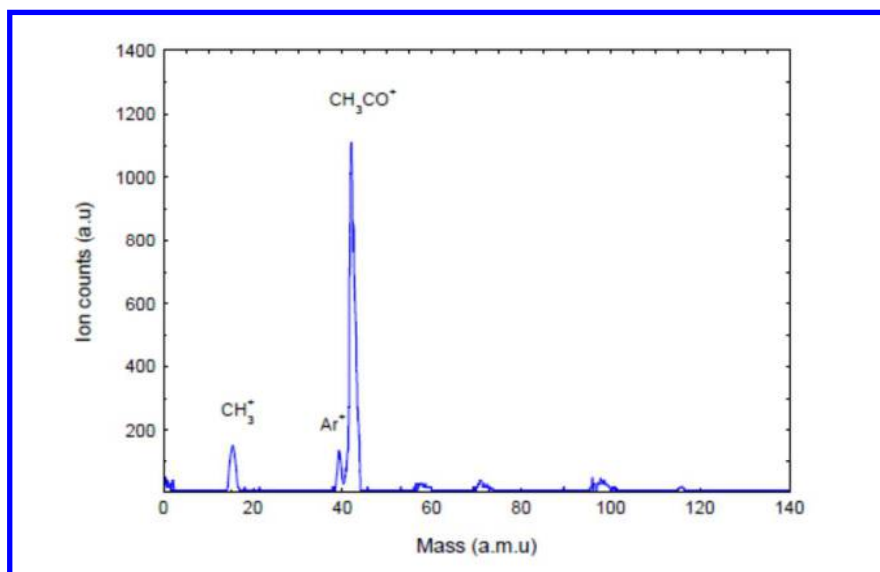


Fig. 3: Mass spectrum taken 30 mm downstream from the final injection port following injection of the helium/acetone mixture into the Ar^+ dominated plasma to produce a neutral acetone density of $3.2 \times 10^{12} \text{ cm}^{-3}$. Chamber pressure 0.53Torr;

Although CH_3CO^+ is highly dominant in the plasma, however, there are also other molecular ions and so the multiple ion / z variable method as described by equation (6), was used to derive the rate coefficient. The measurements were repeated several times and a typical result is shown in figure 4.

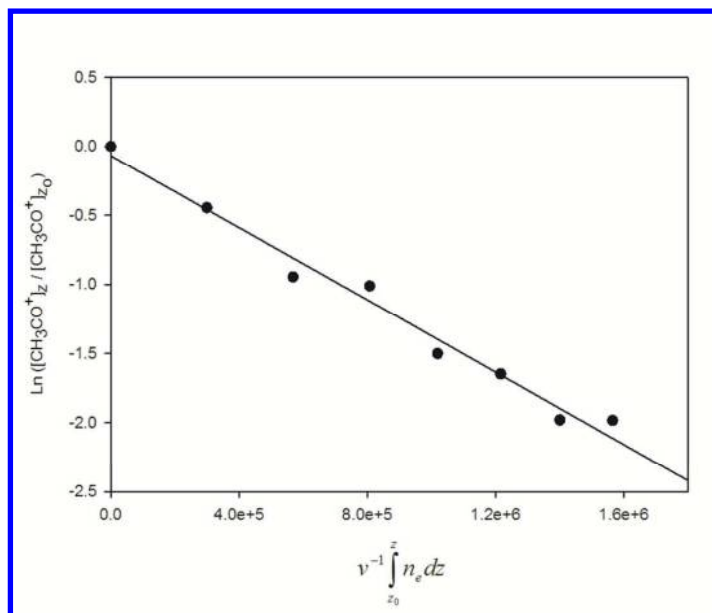
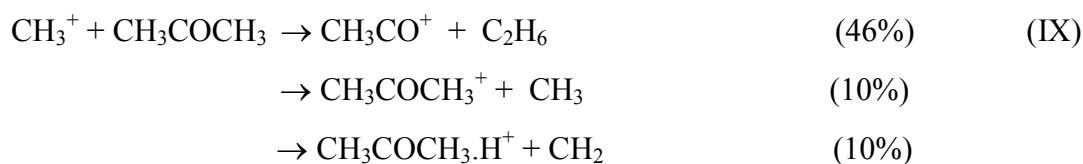


Fig. 4. Plot of the logarithm of the CH_3CO^+ signal at position z over the signal at the origin, z_0 as a function of the integral over the distance of the electron density. The slope multiplied by the flow velocity ($v=1.85 \times 10^4 \text{ cm.s}^{-1}$) yields the recombination rate coefficient.

The value obtained for the DR rate coefficient for CH_3CO^+ using this method, was $1.29 \pm 0.15 \times 10^{-6} \text{ cm}^3 \text{ s}^{-1}$. This is certainly a high value for what is not a very complex ion but can be compared with other polyatomic ions¹ such as CH_3NH_3^+ ($1.4 \times 10^{-6} \text{ cm}^3 \text{ s}^{-1}$), or $\text{CH}_3\text{SSHCH}_3^+$ ($1.48 \times 10^{-6} \text{ cm}^3 \text{ s}^{-1}$). One of the major problems with dissociative recombination, is that there is no real understanding of the effect of complexity on the recombination rate and there seems to be no real trend from one ion to another.

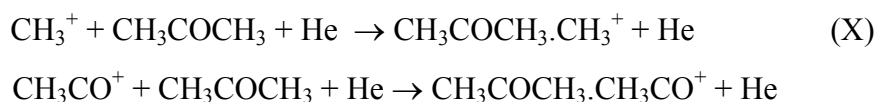
3.2 Medium acetone density

When the flow rate of the He/acetone mixture was increased to yield an acetone molecule density in the flow of $2.3 \times 10^{13} \text{ cm}^{-3}$, a much more complex spectrum was found (Figure 6) with the acetone ion $\text{CH}_3\text{COCH}_3^+$, the adduct ions ($\text{CH}_3\text{COCH}_3 \cdot \text{CH}_3^+$ and $\text{CH}_3\text{COCH}_3 \cdot \text{CH}_3\text{CO}^+$ and the cluster ion $(\text{CH}_3\text{COCH}_3)_2^+$. This is because the two primary ions seen to be formed at low acetone densities, go on to react with the acetone molecules once the latter are present in higher concentration. It is interesting to note that the acetone parent ion is now seen to be present in the spectrum. CH_3CO^+ is still in a significant proportion but CH_3^+ has disappeared. Indeed, measurements²⁵ have shown that CH_3^+ reacts with acetone via the reactions (IX):



The mass resolution of the spectrometer used in this experiment is not sufficient to distinguish between the parent ion and protonated acetone so it must be assumed that both are present in the spectrum shown in figure 6.

The adduct ions are formed via the three-body association reactions (X)



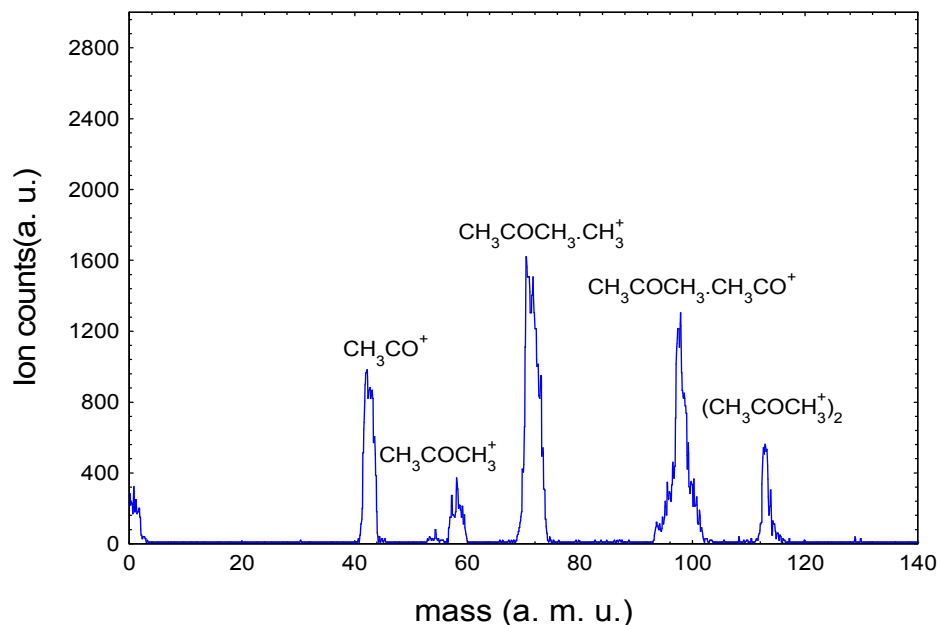


Fig. 5: Mass spectrum taken 30 mm downstream from the final injection port following injection of the He/acetone mixture into plasma dominated by Ar^+ a flow rate yielding an acetone density of $(2.3 \times 10^{13} \text{ molecules.cm}^{-3})$. Chamber pressure was 0.55 Torr.

Figures 6, 7 and 8 show the ratio of $CH_3COCH_3^+$, $(CH_3COCH_3) \cdot CH_3^+$ and $(CH_3COCH_3) \cdot CH_3CO^+$ ion densities respectively, measured downstream at z , to the corresponding densities at the origin $z_0 = 30 \text{ mm}$, plotted at various z values between 30 and 100 mm, against the integral of the electron density divided by the flow velocity. The experiment was repeated several times and using this method, the following average values of the dissociative recombination rate coefficients for these ions were obtained. $CH_3COCH_3^+$ ($2.6 \pm 0.3 \times 10^{-6} \text{ cm}^3\text{s}^{-1}$), $CH_3COCH_3^+ \cdot CH_3^+$ ($2.25 \pm 0.1 \times 10^{-6} \text{ cm}^3\text{s}^{-1}$) and $CH_3COCH_3^+ \cdot CH_3CHO^+$ ($2.3 \pm 0.35 \times 10^{-6} \text{ cm}^3\text{s}^{-1}$).

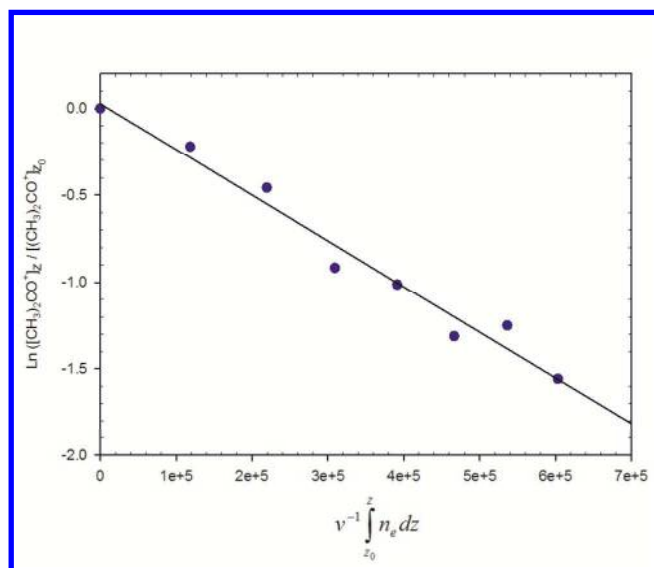


Fig. 6: The ratio of $CH_3COCH_3^+$ ion density measured downstream to that at origin plotted against the integral of the electron density divided by the flow velocity.

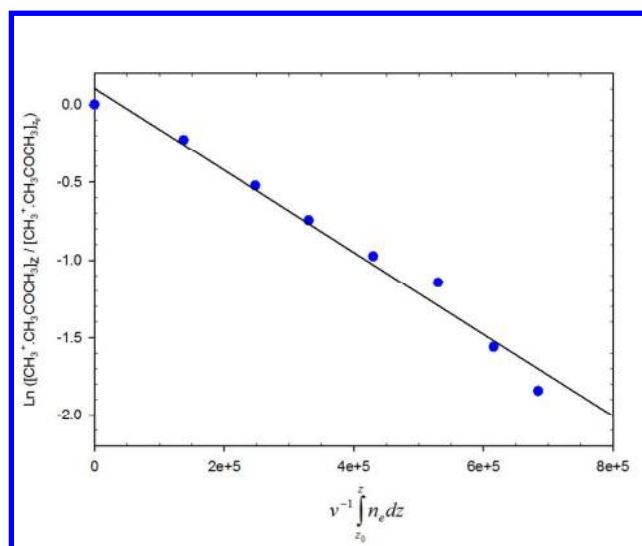


Fig. 7: The ratio of $(CH_3COCH_3).CH_3^+$ ion density measured downstream to that at origin plotted against the integral of the electron density divided by the flow velocity.

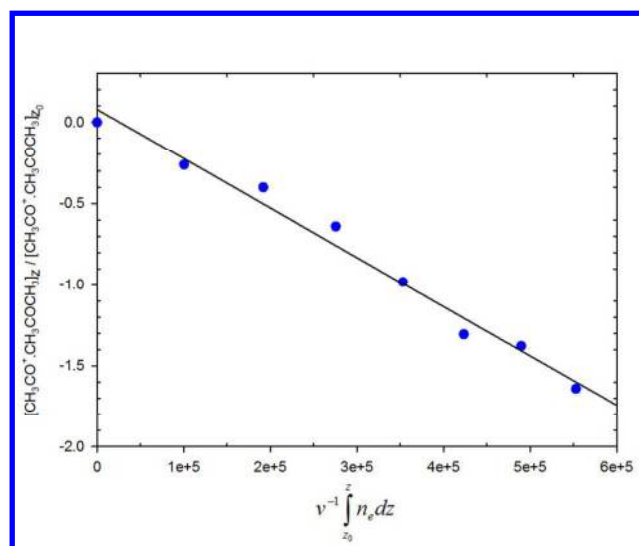


Fig. 8: The ratio of $(CH_3COCH_3).CH_3CO^+$ ion density measured downstream to that at origin plotted against the integral of the electron density divided by the flow velocity.

The measurements just described are valid under the conditions where ion-molecule reactions, leading to the production or destruction of these ions can be ignored. Indeed these processes would contribute to there being a difference in the measured number densities as a function of distance z along the flow and given the complexity of the situation here (aggregation, adduct formation), an alternative approach was used to eliminate this problem. Ratios of the number densities for these ions at a fixed given point z , to those at an arbitrarily chosen point $z=0$, were measured for different electron densities. This is the multiple ion/fixed z method. Since the

change in the ratio of these number densities due to ion-molecule reactions is independent of the electron density, then the latter can be ignored, whether they are responsible for production or destruction.

The electron density in the plasma could be changed by varying the position of the microwave cavity with respect to the position of the helium gas inlet tube, G1 (see figure 1). The measurements illustrated in figures 9, 10, 11 were made in this way.

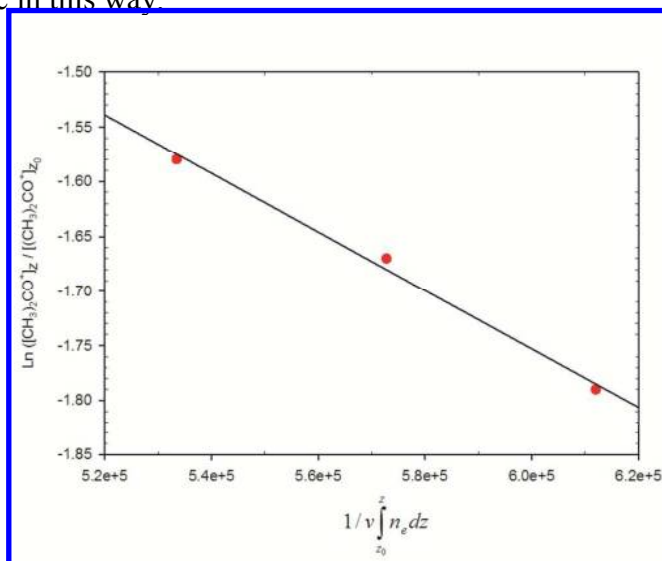


Fig. 9: The ratio of the density of CH_3COCH^+ at a single value of $z = 100$ mm downstream from the origin to the density at z_0 vs the integral of the electron density from z_0 to z , for three different initial electron densities, 2.8, 3.2, 5.7 $\times 10^9 \text{ cm}^{-3}$

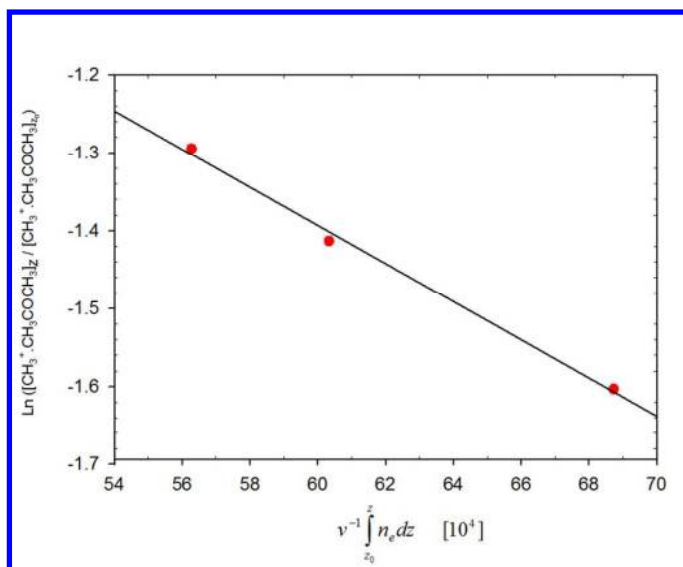


Fig. 10: The ratio of the density of $(\text{CH}_3\text{COCH}_3).\text{CH}_3^+$ at a single value of $z = 100$ mm downstream from the origin to the density at z_0 vs the integral of the electron density from z_0 to z , for three different initial electron densities, 2.8, 3.2, 5.7 $\times 10^9 \text{ cm}^{-3}$.

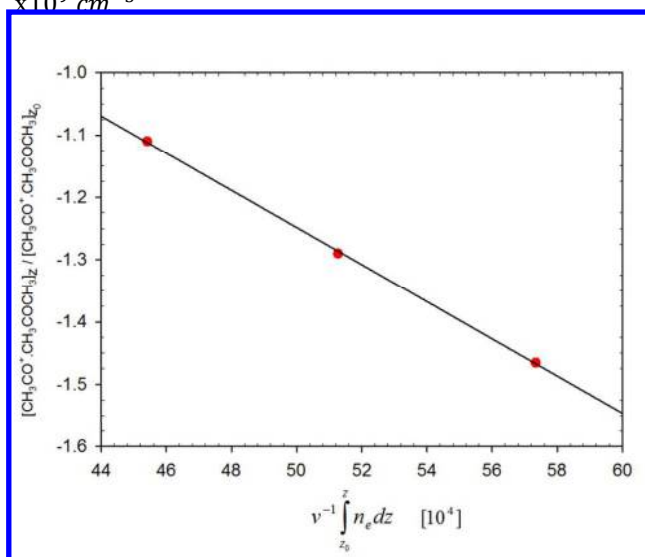


Fig. 11: The ratio of the density of $(\text{CH}_3\text{COCH}_3).\text{CH}_3\text{CO}^+$ at a single value of $z = 100$ mm downstream from the origin to the density at z_0 vs the integral of the electron density from z_0 to z , for three different initial electron densities, 2.8, 3.2, 5.78 $\times 10^9 \text{ cm}^{-3}$.

1
2
3 With the multiple ion / fixed z method, the following values were found: $\text{CH}_3\text{COCH}_3^+$ (2.7×10^{-6}
4 cm^3s^{-1}), $\text{CH}_3\text{COCH}_3^+ \cdot \text{CH}_3^+$ (2.4×10^{-6} cm^3s^{-1}) and $\text{CH}_3\text{COCH}_3^+ \cdot \text{CH}_3\text{CHO}^+$ (2.9×10^{-6} cm^3s^{-1}), i.e.
5 very close to those obtained with the multiple ion/z variable method.
6

7
8 As far as we know, there have been no other measurements of recombination of these ions and
9 indeed no measurements of the recombination of adduct ions. The latter are also known as
10 “pseudomolecules” and are often found in the mass spectra of polyatomic ions. They are distinct
11 from cluster ions as the attached functional groups are bound to the parent molecule by hydrogen
12 bonds and thus are much more stable than cluster ions which are bound by polarization forces.
13

14
15 It is interesting to speculate why the two measurement methods have such close agreement even
16 though the multiple ion/fixed Z approach should be more precise. In fact examination of
17 equation (7) yields a clue to this since, if $[\text{A}^+]$ and $[\text{M}^+]$ are not too different and if we can
18 assume that the ion molecule reactions involved in the formation and destruction of $[\text{M}^+]$ are not
19 too different (granted that the branching ratios for the products are not well known), then the
20 production and destruction terms will tend to cancel each other out. This argument could apply to
21 CH_3CO^+ which when there are no longer any Ar^+ in the plasma, is formed by the reaction of
22 CH_3^+ with acetone (reaction IX) but then reacts further with acetone to form the corresponding
23 adduct (reaction X). For the CH_3^+ -acetone adduct, the situation is different as it can be seen in
24 figure 5 that under these conditions, CH_3^+ is exhausted, having been used up in forming its
25 adduct. As we shall see in the next section, the adducts themselves are not terminal ions in the
26 sense that they can undergo further reaction if there is sufficient acetone density. It should be
27 remembered however, that the formation process is a three-body reaction and the reaction of
28 these adducts to form dimer ions is not known. It may just be that the high recombination rate
29 found, dominates the ion chemistry under these acetone density conditions
30
31
32
33

34 *3.3 High density of acetone*

35
36 For a moderate acetone density, a large signal was found for the clusters ions $(\text{CH}_3\text{COCH}_3)_2^+$ but
37 the decay of its signal along the flow was not seen. In fact the signal was found to rise with
38 increasing z. This is because this ion is continually formed by the reaction of acetone ions with
39 neutral acetone molecules, and indeed reactions of the adduct ions with acetone. Going to a
40 much higher flow rate of acetone mixture (the acetone density was roughly 5.8×10^{13} cm^{-3}),
41 yielded the spectrum shown in fig. 12. It is seen that now there is only one ion in the plasma
42 under this condition. Because of this, the rate coefficient could be determined by using the single
43 ion method based on equation 4 (fig. 13) and an average value of 1.45×10^{-6} cm^3s^{-1} was
44 obtained.
45
46
47
48
49
50
51
52
53
54
55
56
57
58
59
60

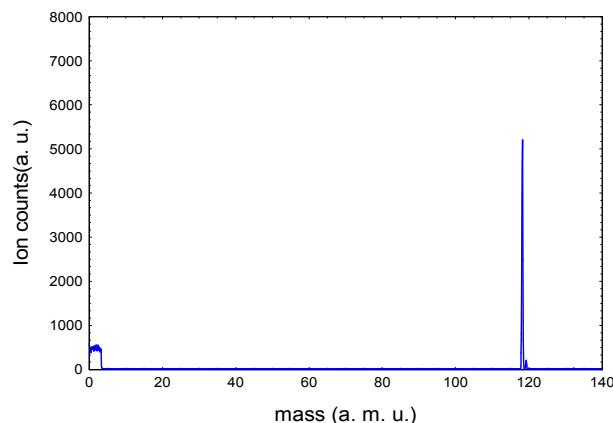


Fig. 12: Mass spectrum taken 30 mm downstream from the final injection port following injection of acetone mixture ($5.8 \times 10^{13} \text{ cm}^{-3}$) into an Ar^+ dominated plasma.

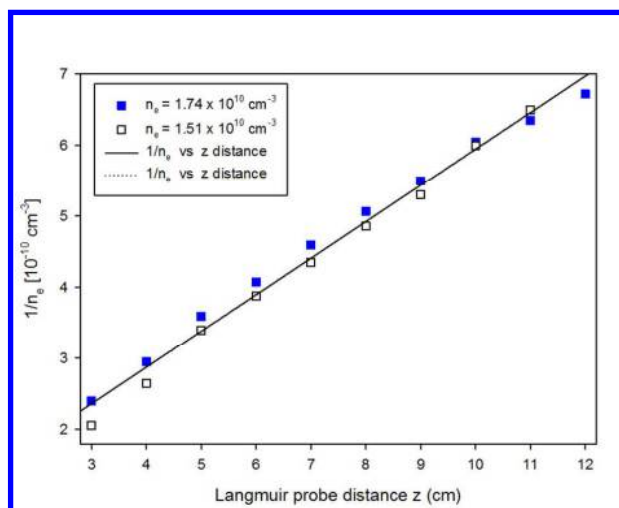


Fig. 13: A plot of the inverse of the electron density vs distance downstream for an afterglow formed from CH_3COCH_3 for two initial electron densities. The rate coefficient is obtained directly from the slope, given by α/v .

Glosik and Plasil²⁶ did measure the recombination rate for the protonated form of the ion in a high pressure (5 Torr) flowing-afterglow apparatus. In their experiment, proton transfer reaction was used to create protonated acetone clusters. They found a value of $3.4 \times 10^{-6} \text{ cm}^3 \text{ s}^{-1}$ at $T_e = 580\text{K} \pm 150 \text{ K}$ and 7×10^{-6} at $T_e = 450 \pm 100 \text{ K}$. These values are much higher than what we have found here and indeed seem to be unreasonably high, implying a value of about $10^{-5} \text{ cm}^3 \text{ s}^{-1}$ at 300K.

4 Conclusion

Finally, table 2 presents a summary of the values obtained for these ions using these different methods.

Ion	Single ion method ($10^{-6} \text{ cm}^3 \text{ s}^{-1}$)	Multiple ions/z-variable (Electron density fixed) ($10^{-6} \text{ cm}^3 \text{ s}^{-1}$)	Multiple ions/z fixed Electron density variable ($10^{-6} \text{ cm}^3 \text{ s}^{-1}$)
CH_3CO^+	N/A	1.29	
$\text{CH}_3\text{COCH}_3^+$	N/A	2.6 ± 0.3	2.7
$\text{CH}_3^+ \cdot \text{CH}_3\text{COCH}_3$	N/A	2.5 ± 0.1	2.4
$\text{CH}_3\text{CO}^+ \cdot \text{CH}_3\text{COCH}_3$	N/A	2.6 ± 0.35	2.9

$(\text{CH}_3\text{COCH}_3)_2^+$	1.45±0.1		
----------------------------------	----------	--	--

Table 1. Summary of measured recombination rates determined using the three different methods discussed in the text.

The unique ability of the FALP-MS apparatus, allows a plasma containing several ions to be treated and the recombination rates of the individual ions to be determined. Several methods have been used and it is interesting to note in Table 1 that the values obtained are consistent for a given ion. This indicates that under the conditions studied, the destruction of the ions by recombination dominates, with the exception of the dimer ion where this is only true at high acetone densities.

The values measured are generally rapid as seen for many other ions¹ but there is no systematic dependence of this value on ion complexity. Barring a couple of exceptions (He_2^+ , ArH^+), dissociative recombination rates¹ general fall into a rather narrow range from about 1×10^{-7} to $5 \times 10^{-6} \text{ cm}^3\text{s}^{-1}$. (This can be compared to the sister reaction of electron attachment to neutrals where rates vary over about 5 or 6 orders of magnitude). The values obtained for the recombination rate for the adduct ions and the dimer, are in line with other measurements of hydrocarbon dimer ions¹ (e.g. $(\text{CH}_3\text{COH})_2\text{H}^+$, $\alpha = 1.4 \times 10^{-6} \text{ cm}^3\text{s}^{-1}$). Our value for the acetone dimer is much lower than that found by Glosik and Plasil²⁶ but their measurement was at a pressure an order of magnitude higher than ours and it is possible that three body recombination effects may have played a role in that experiment.

In this study, we have demonstrated that it is possible with our FALP-MS apparatus, to measure the recombination rate coefficients under plasma conditions where there are multiple ions and where these ions are not terminal ions, but where production and destruction via ion-molecule reactions play a role in the decay processes.

AUTHOR INFORMATION

Author Contributions

mitchell@univ-rennes1.fr

The manuscript was written through contributions of all authors. All authors have given approval to the final version of the manuscript. The authors declare no competing financial interest.

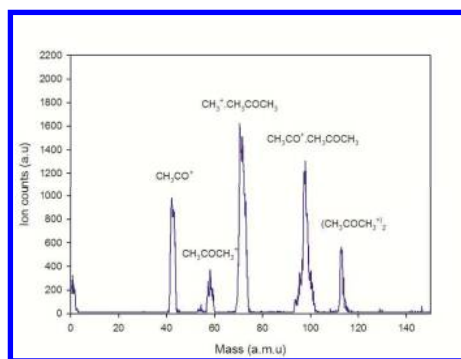
Acknowledgments: S. Al Shammari would like to thank the King Abdulaziz City for Science and Technology for funding his thesis work which underlies this paper.

REFERENCES

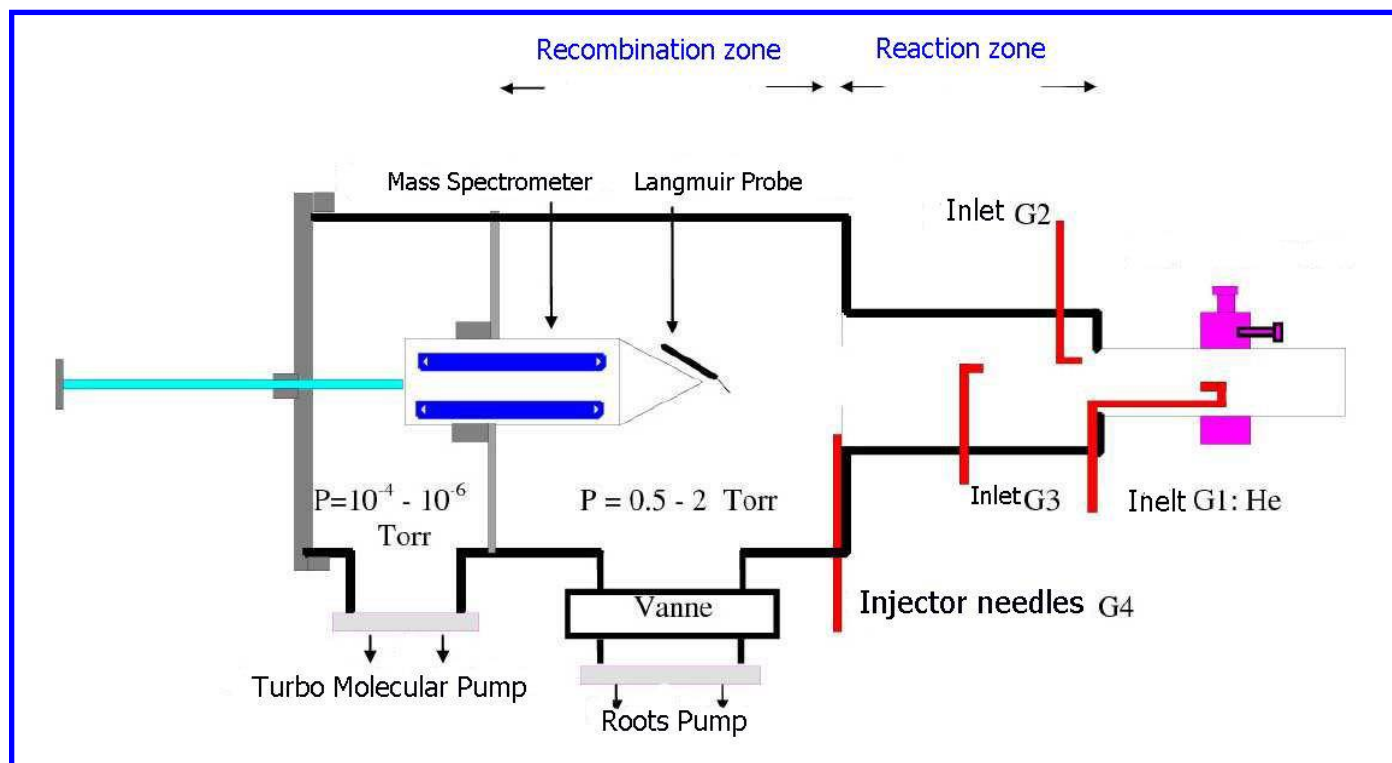
(1) Florescu-Mitchell, A.I. and Mitchell, J. B. A. Dissociative recombination, *Phys. Rep.* **2006**, *430*, 277–374.

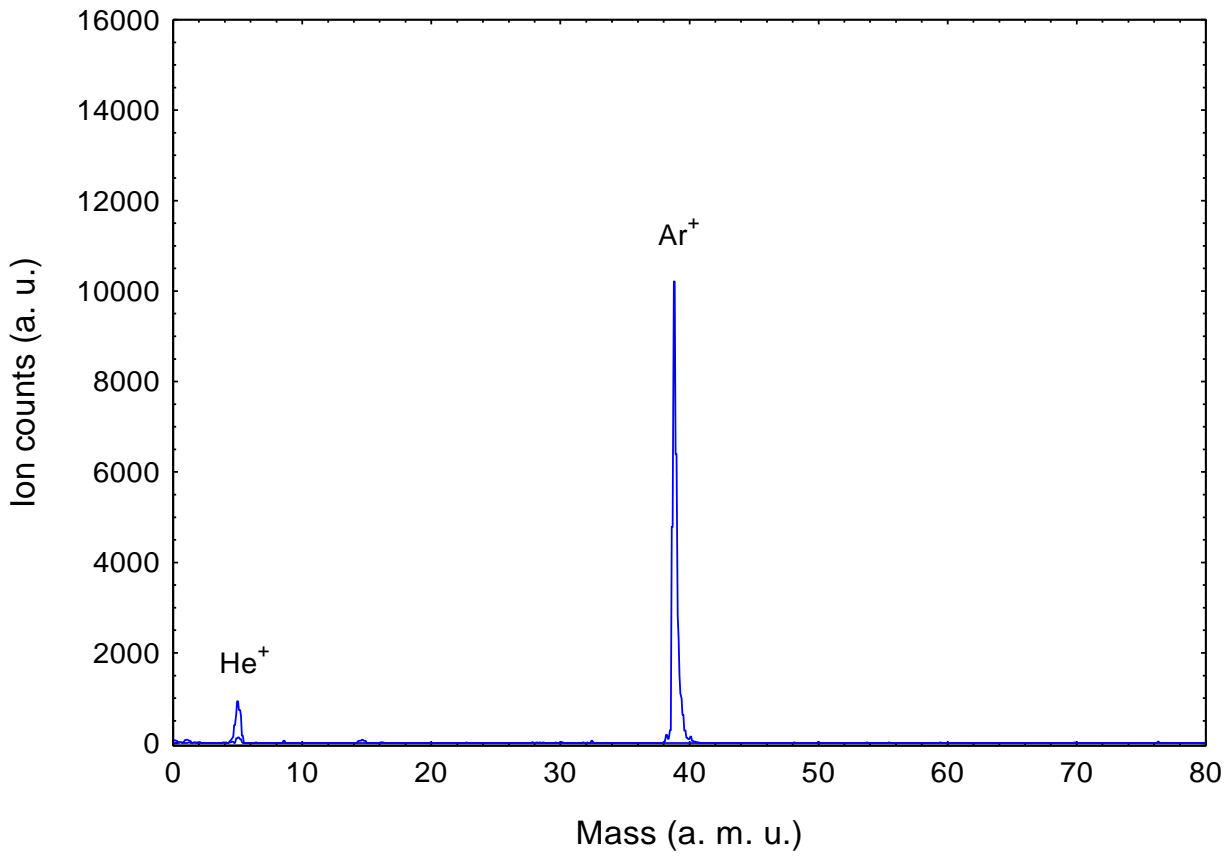
- 1
2
3 (2) Larsson, M. and Orel, A. E. *Dissociative Recombination of Molecular Ions*, Cambridge
4 University Press, Cambridge, 2008.
5
6 (3) Adams, N.G. and Smith, D. Measurements of the dissociative recombination coefficients for
7 several polyatomic ion species at 300 K, *Chem. Phys. Letters* **1998**, *144*, 11-14.
8
9 (4) Combes, F.; Gerin, M.; Wootten, A.; Wlodarczak, G.; Clausset, F.; Encrenaz, P. J. Acetone in
10 interstellar space, *Astron. Astrophys.* **1987**, *180*, L13-L16.
11
12 (5) Friedel, D. N.; Snyder, L. E.; Remijan, A. J.; Turner, B. E. Detection of interstellar acetone
13 towards the Orion-K1 hot core, *Astrophys. J.* **2005**, *632*, L95-L98.
14
15
16 (6) Herbst, E.; Giles, K.; Smith, D. Is interstellar acetone produced by ion-molecule chemistry?
17 *The Astrophysical Journal*, **1990**, *358*, 468-472.
18
19 (7) Millar, T. J.; Herbst, E.; Charnley, S. B. The formation of oxygen-containing organic
20 molecules in the Orion compact ridge, *Astrophys. J.* **1991**, *369*, 147-156.
21
22
23 (8) Ehrenfreund, P.; Charnley, S. B. Organic Molecules in the Interstellar Medium, Comets, and
24 Meteorites: A Voyage from Dark Clouds to the Early Earth, *Annu. Rev. Astron. Astrophys.* **2000**,
25 *38*, 427-483.
26
27 (9) Smith, D. and Spanel, P. Swarm Techniques in *Experimental Methods in the Physical*
28 *Sciences*, Academic Press, Orlando, **1995**, Vol. 29A, p. 273.
29
30
31 (10) Gougousi, T.; Johnsen, R. and Golde, M.F. Recombination of H_3^+ and D_3^+ ions in a
32 flowing afterglow plasma, *Int. J. Mass Spec. and Ion Proc.* **1995**, *149-150*, 131-151.
33
34 (11) Adams, N.G. Afterglow techniques with spectroscopic detection for determining the
35 rate coefficients and products of dissociative electron-ion recombination, *Int. J. Mass Spec.*
36 *and Ion Proc.* **1994**, *132*, 1-27.
37
38
39 (12) Novotny, O.; Plasil, R.; Pysanencko, A.; Korolov, I.; Glosik, J. The recombination of
40 D_3^+ and D_5^+ ions with electrons in deuterium containing plasma *J. Phys. B: At. Mol. Opt.*
41 *Phys.* **2006**, *39*, 2561-2544.
42
43 (13) Almeida, G.C.; Pilling, S.; Andrade, D.P.P.; Castro, N. S.; Mendoza, E.; Boechat-Roberty,
44 H. M.; Rocco, M. M. Photodesorption and photostability of acetone ices: Relevance to solid
45 phase astrochemistry, *J. Phys. Chem. C* **2014**, *118*, 6193-6200.
46
47 (14) Ferguson, E.E.; Fehsenfeld, F.C. and Schmeltekopf, A.L. Flowing afterglow measurements
48 of ion-neutral reactions, *Adv. Mol. Phys.* **1969**, *5*, 1-56.
49
50
51 (15) Adams, N.G.; Smith, D.; Alge, E. Measurements of dissociative recombination
52 coefficients of H_3^+ , HCO^+ , N_2H^+ , and CH_5^+ at 95 and 300 K using the FALP apparatus, *J. Chem.*
53 *Phys.* **1984**, *81*, 1778-1784.
54
55
56
57
58
59
60

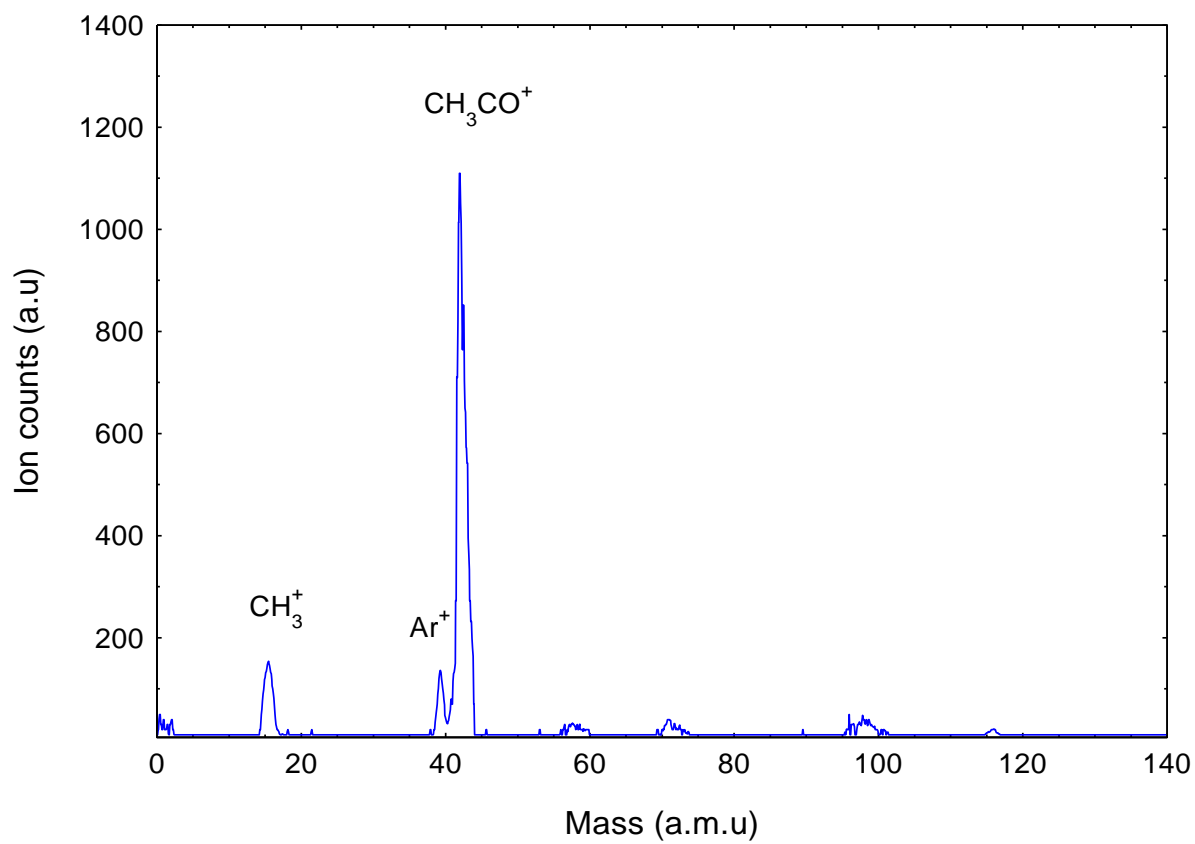
- 1
2
3 (16) Mahdavi M. R.; Hasted, J.B.; Nakshbandi, M.M. Electron-ion recombination measurements
4 in the flowing afterglow, *J. Phys. B: Atom. Molec. Phys.* **1971**, *4*, 1726.
5
6 (17) Fournier J.A.; Shuman N.S.; Melko J.J.; Ard S.G.; Viggiano A.A. A novel technique for
7 measurement of thermal rate constants and temperature dependences of dissociative
8 recombination: CO_2^+ , CF_3^+ , N_2O^+ , C_7H_8^+ , C_7H_7^+ , C_6H_6^+ , C_6H_5^+ , C_5H_6^+ , C_4H_4^+ and C_3H_3^+ , *J.*
9 *Chem. Phys.* **2013**, *138*, 154201-7.
10
11 (18) Lehfaoui, L.; Rebrion-Rowe, C.; Rowe, B.R.; Mitchell, J.B.A. The dissociative
12 recombination of hydrocarbon ions: I Light alkanes”, *J. Chem. Phys.* **1997** *106*, 5406.5412.
13
14 (19) Mostefaoui, T.; Laube, S.; Gautier, G.; Rebrion-Rowe, C.; Rowe, B.R.; Mitchell, J.B.A. The
15 dissociative recombination of NO^+ : the influence of the vibrational excitation state, *J. Phys. B.*
16 **1999**, *32*, 5247.
17
18 (20) Le Garrec, J-L. Étude de processus physico-chimiques d'intérêt pour la physique des
19 plasmas et la combustion, HDR Thesis, Université de Rennes I, 2008.
20
21 (21) Rowe, B.R.; Canosa, A. and Le Page, V. FALP and CRESU studies of ionic reactions *Int. J.*
22 *Mass Spectrom. Ion Proc.* **1995**, *149/150*, 573-596.
23
24 (22) Y.S. Ikezoe, M. Matsuoka, M. Takebe; A.A. Viggiano *Gas Phase Ion-Molecule Reaction*
25 *Rate Constants Through 1986*, Maruzen, Japan, 1987
26
27 (22) Rebrion-Rowe, C.; Lehfaoui, L.; Rowe, B.R.; Mitchell, J.B.A. “The dissociative
28 recombination of hydrocarbon ions: II Alkene and alkyne derived species”, *J. Chem. Phys.*,
29 **1998**, *108*, 7185-7189.
30
31 (23) Prabhudesai, V.S.; Tadsare, V.; Ghosh, S.T.; Gope, K.; Davis, D.; Krishnakumar, E.
32 Dissociative electron attachment studies on acetone, *J. Chem. Phys.* **2014**, *141*, 164320
33
34 (24) MacNeil, K.A.G. and Futrell, J.H. Ion-molecule reactions in gaseous acetone, *J. Phys.*
35 *Chem.* 1972, *76*, 409-415.
36
37 (25) Glosik, J. and Plasil, R. The recombination rate coefficient of a protonated acetone
38 dimer with electrons: indication of a temperature dependence, *J. Phys. B: At. Mol. Opt. Phys.*
39 **2000**, *33*, 4483–4493.
40
41 (29) Mitchell, J.B.A. and Rebrion-Rowe, C. The recombination of electrons with complex
42 molecular ions, *Int. Rev. Phys. Chem.* **1997**, *16*, 201-213.
43
44
45
46
47
48
49
50
51
52
53
54
55
56
57
58
59
60



TOC Graphic







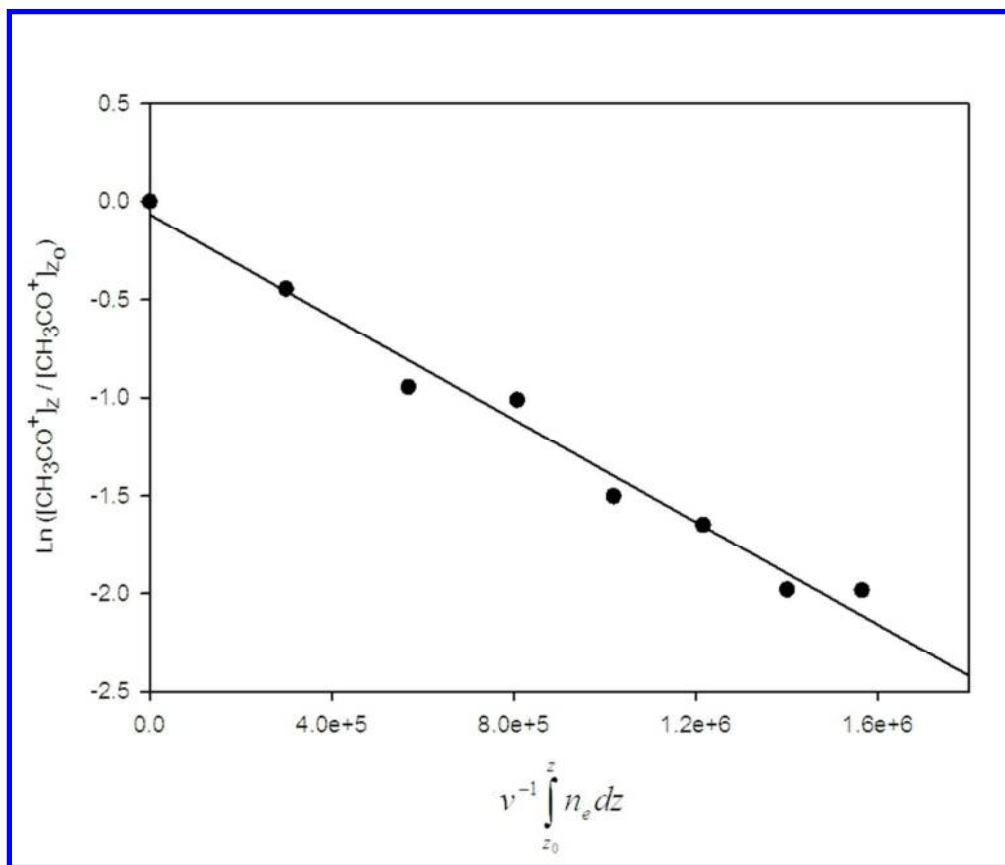


Fig. 4. Plot of the logarithm of the CH₃CO⁺ signal at position z over the signal at the origin, z₀ as a function of the integral over the distance of the electron density. The slope multiplied by the flow velocity ($v=1.85 \times 10^4$ cm.s⁻¹) yields the recombination rate coefficient.

152x129mm (150 x 150 DPI)

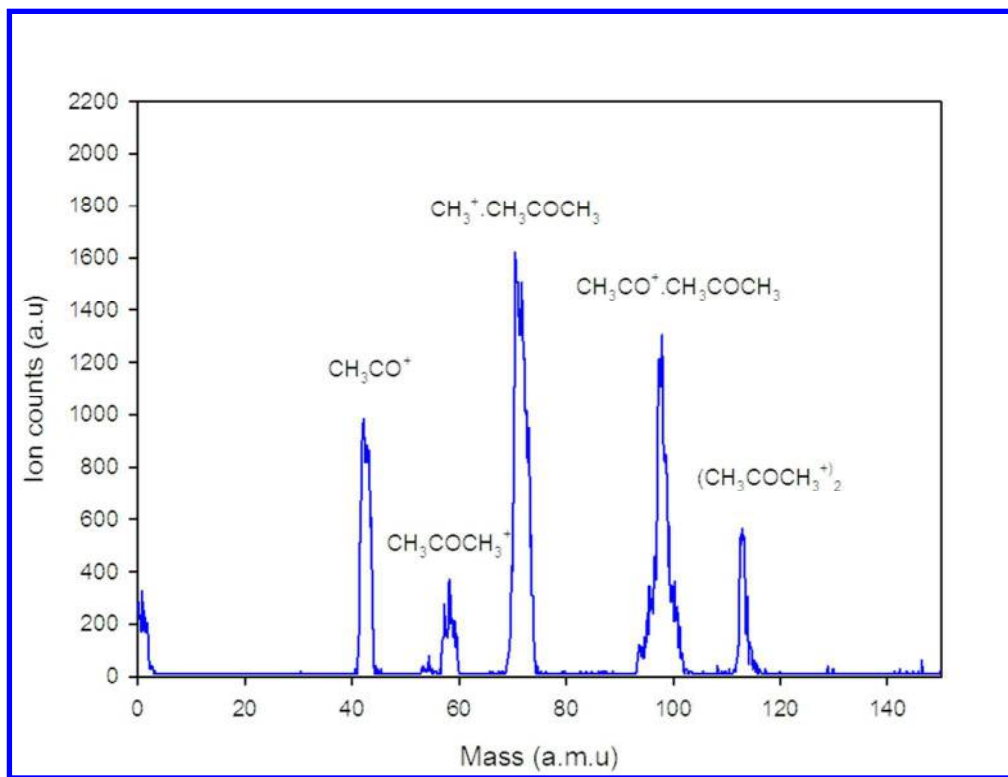


Fig. 5: Mass spectrum taken 30 mm downstream from the final injection port following injection of the He/acetone mixture into plasma dominated by $[\text{Ar}]^+$ a flow rate yielding an acetone density of $(2.3 \times 10^{13} \text{ molecules.cm}^{-3})$. Chamber pressure was 0.55 Torr.

155x118mm (150 x 150 DPI)

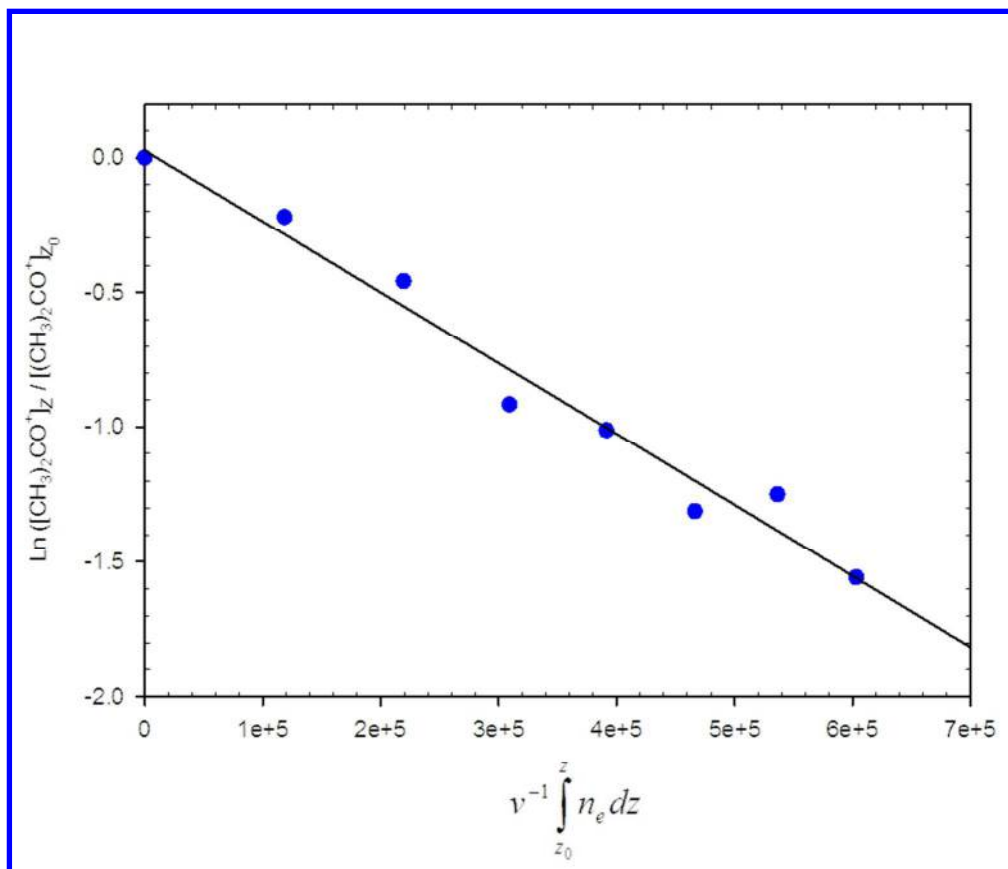


Fig. 6: The ratio of $[\text{CH}_3\text{CO}^+]_z / [\text{CH}_3\text{CO}^+]_{z_0}$ ion density measured downstream to that at origin plotted against the integral of the electron density divided by the flow velocity.

151x129mm (150 x 150 DPI)

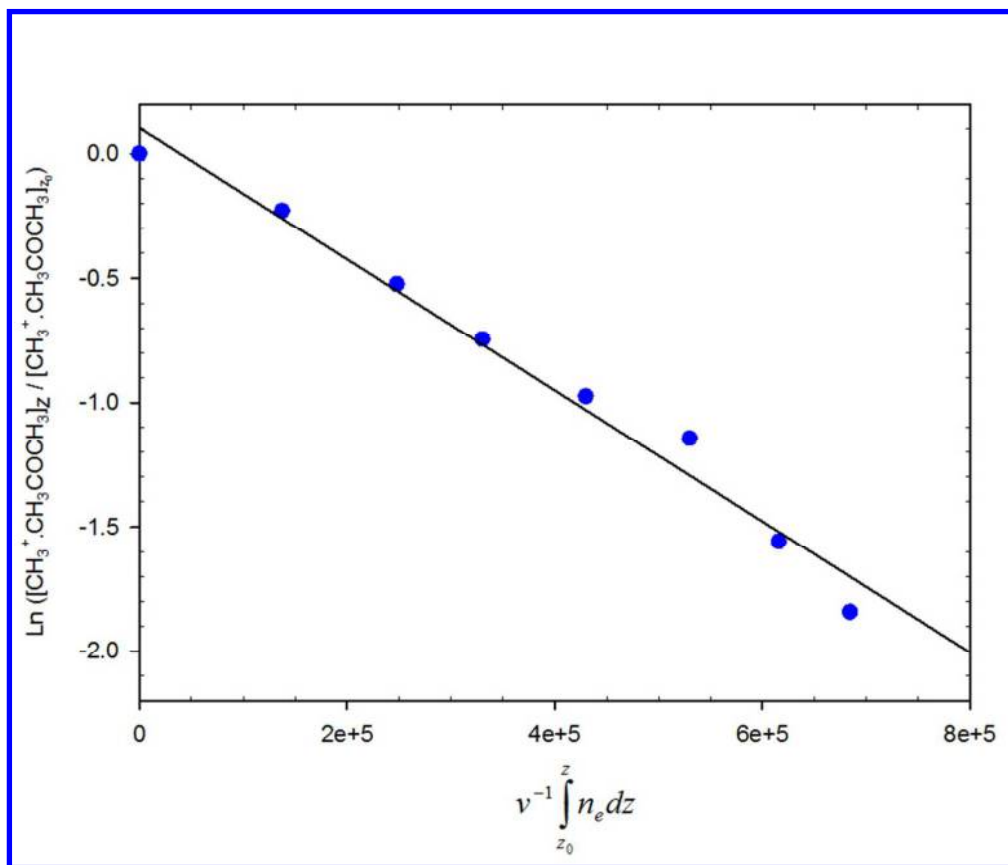


Fig. 7: The ratio of $[(\text{CH})_3 \text{COCH}]_z$, $[(\text{CH})_3^+]$ ion density measured downstream to that at origin plotted against the integral of the electron density divided by the flow velocity.

150x127mm (150 x 150 DPI)

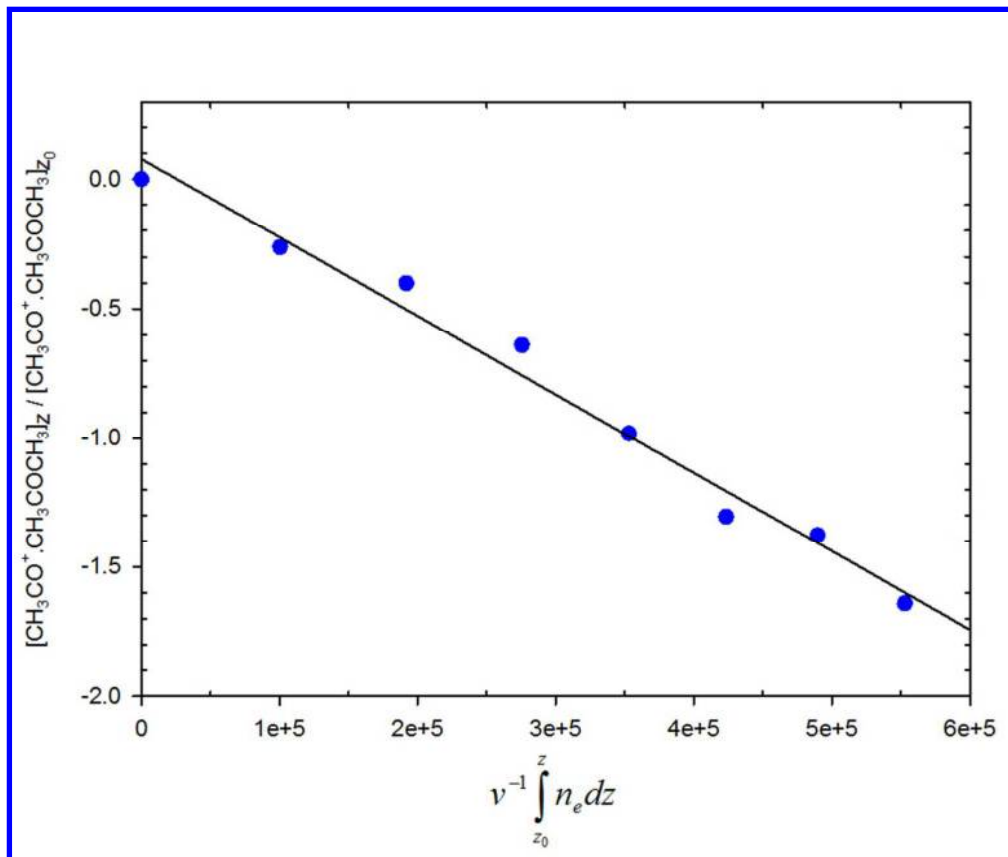


Fig. 8: The ratio of $[(\text{CH})_3 (\text{COCH})_3]$, $[(\text{CH})_3 (\text{CO})^+]$ ion density measured downstream to that at origin plotted against the integral of the electron density divided by the flow velocity.

151x127mm (150 x 150 DPI)

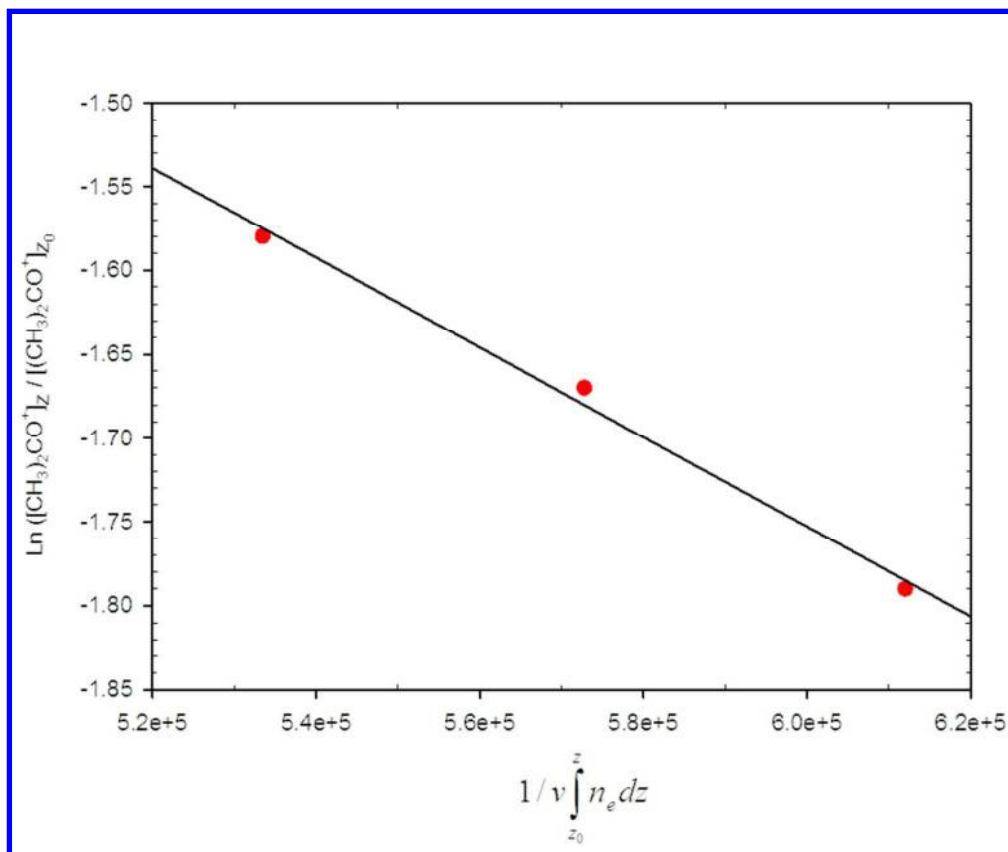


Fig. 9: The ratio of the density of CH_3COCH^+ at a single value of $z = 100$ mm downstream from the origin to the density at z_0 vs the integral of the electron density from z_0 to z , for three different initial electron densities, $2.8, 3.2, 5.7 \times 10^9 \text{ cm}^{-3}$.

153x128mm (150 x 150 DPI)

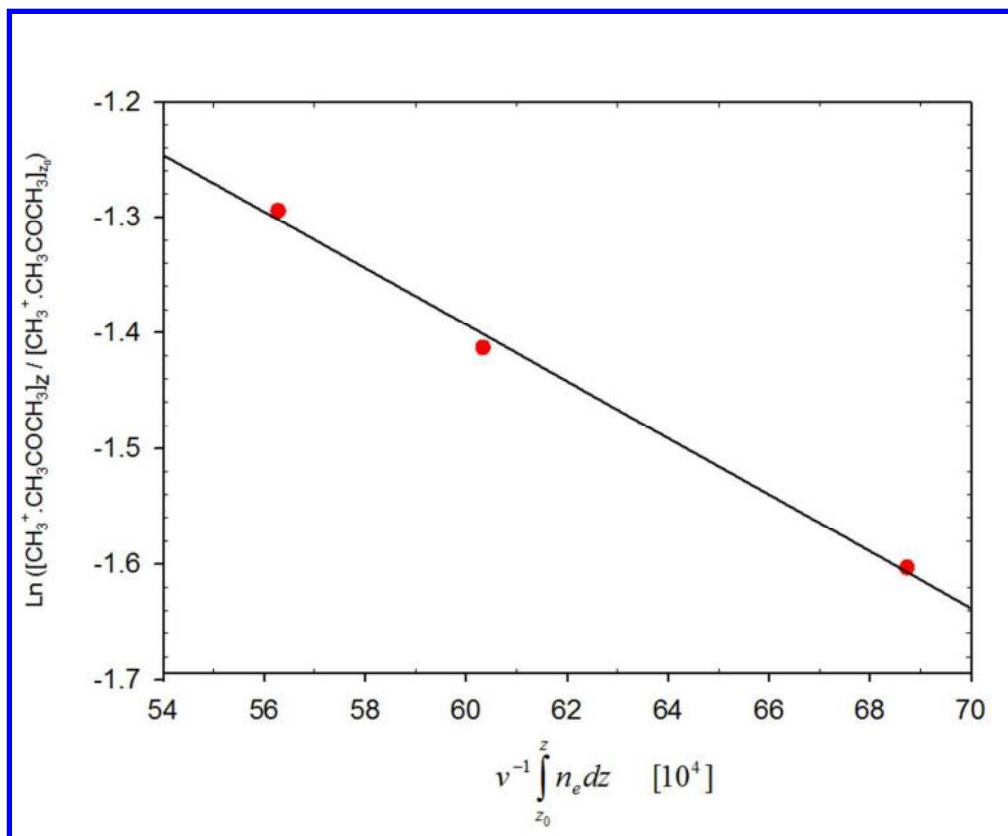


Fig. 10: The ratio of the density of $[(\text{CH})_3 \text{COCH}]_3$, $[(\text{CH})_3^+]$ at a single value of $z = 100$ mm downstream from the origin to the density at z_0 vs the integral of the electron density from z_0 to z , for three different initial electron densities, $2.8, 3.2, 5.7 \times [10]^9 [\text{cm}]^{-3}$.

154x127mm (150 x 150 DPI)

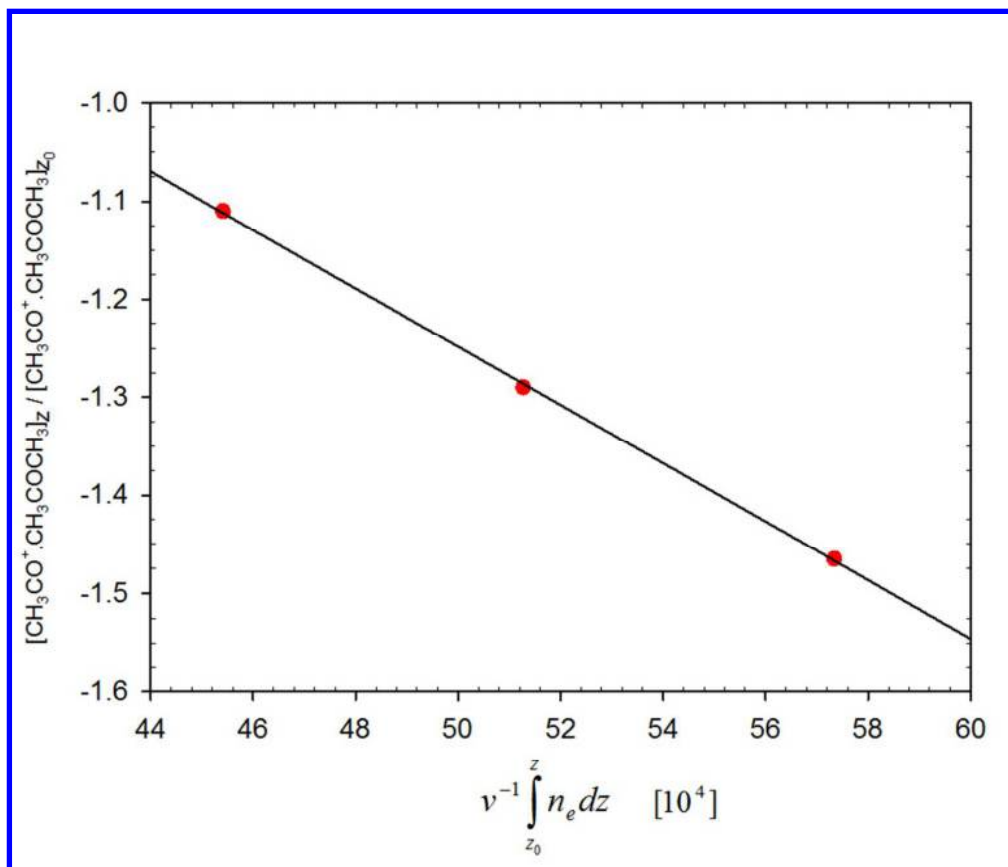
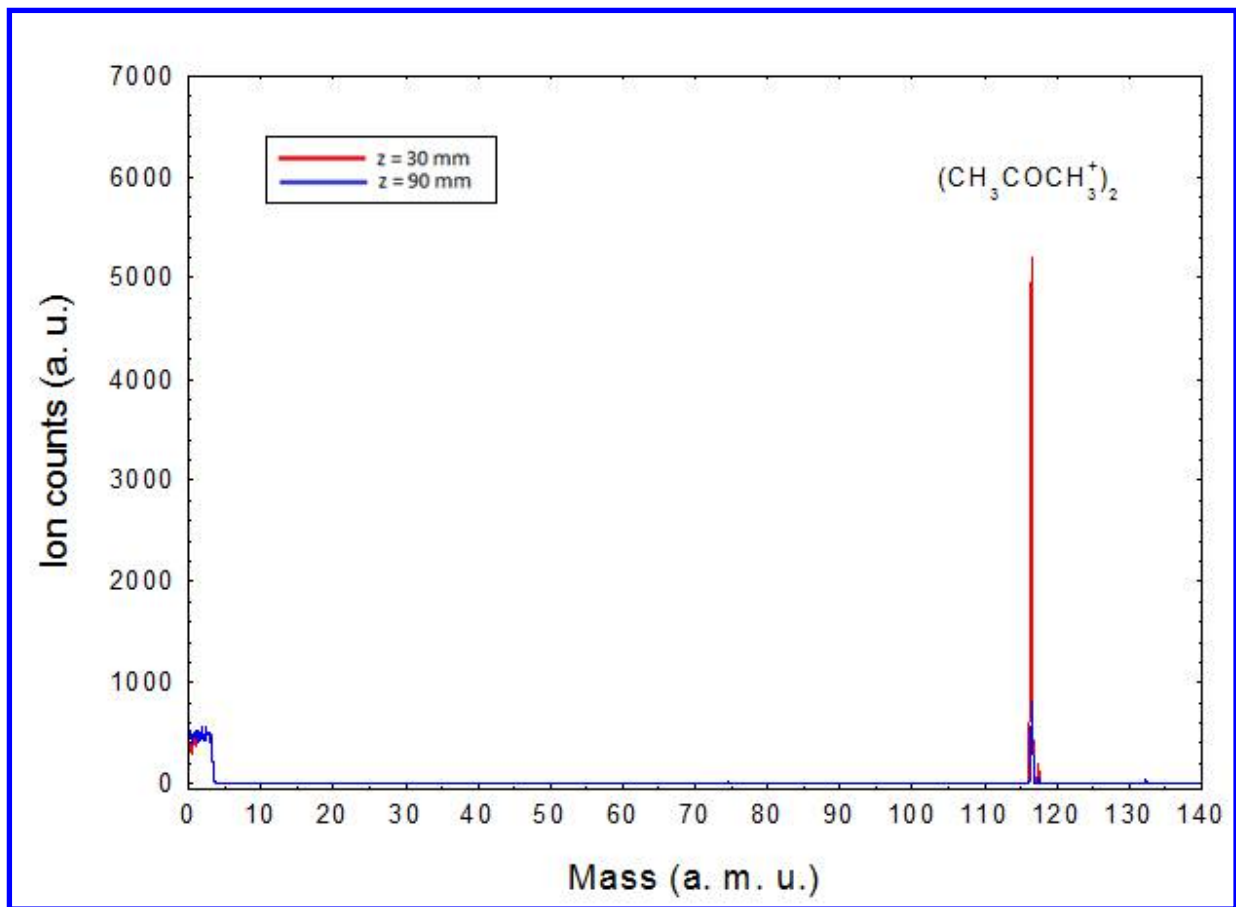


Fig. 11: The ratio of the density of $[(\text{CH})_3(\text{COH})_3]$, $[(\text{CH})_3(\text{CO})^+]$ at a single value of $z = 100$ mm downstream from the origin to the density at z_0 vs the integral of the electron density from z_0 to z , for three different initial electron densities, $2.8, 3.2, 5.78 \times [10]^9 [\text{cm}]^{-3}$.

152x129mm (150 x 150 DPI)



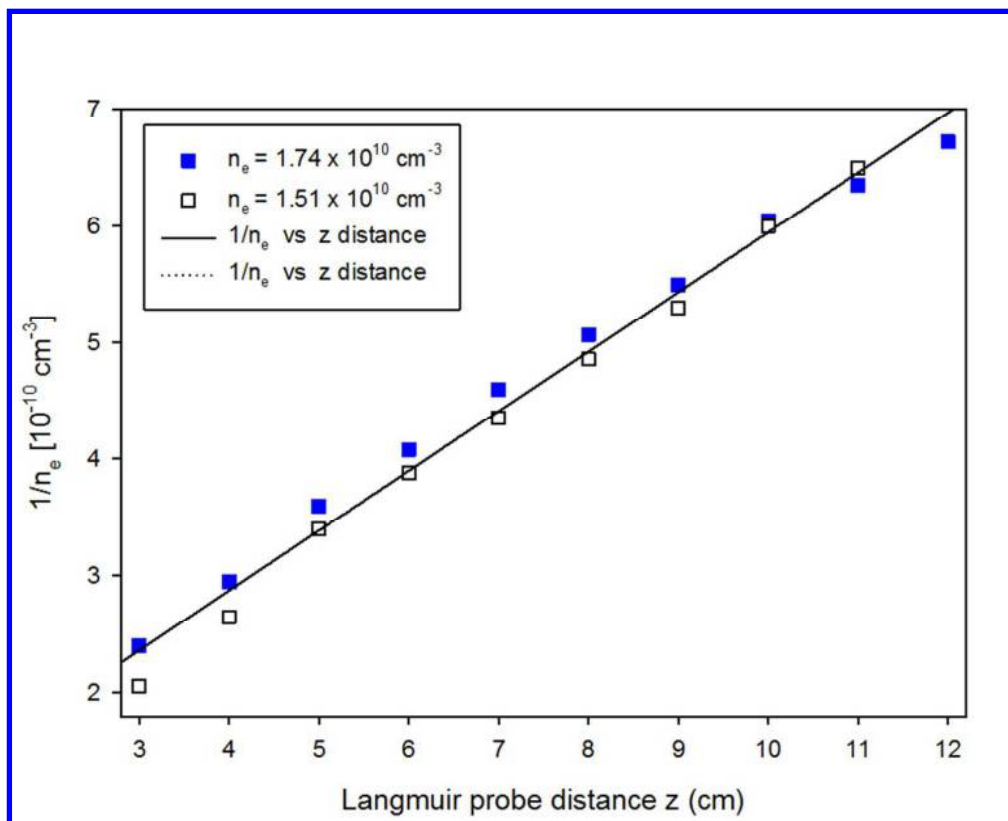


Fig. 13: A plot of the inverse of the electron density vs distance downstream for an afterglow formed from CH_3 for two initial electron densities. The rate coefficient is obtained directly from the slope, given by a/v .

148x119mm (150 x 150 DPI)